Supplemental Information

PDIA3 orchestrates effector T cell program

by serving as a chaperone to facilitate the

non-canonical nuclear import of STAT1 and PKM2

Chun-Liang Yang, Fa-Xi Wang, Jia-Hui Luo, Shan-Jie Rong, Wan-Ying Lu, Qi-Jie Chen, Jun Xiao, Ting Wang, Dan-Ni Song, Jing Liu, Qian Mo, Shuo Li, Yu Chen, Ya-Nan Wang, Yan-Jun Liu, Tong Yan, Wei-Kuan Gu, Shu Zhang, Fei Xiong, Qi-Lin Yu, Zi-Yun Zhang, Ping Yang, Shi-Wei Liu, Decio Eizirik, Ling-Li Dong, Fei Sun, and Cong-Yi Wang
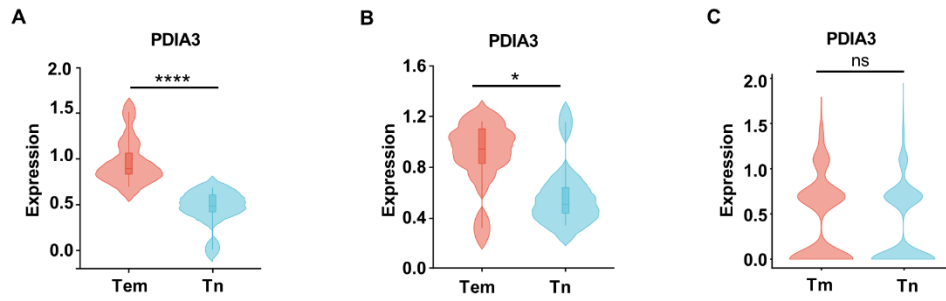
Fig. S1. The expression of *PDIA3* in naïve CD4 T cells and memory CD4 T cells. (A and B) Differential *PDIA3* expression was observed in naïve CD4 T cells (Tn) and effector memory CD4 T cells (Tem) through analysis of bulk RNA-seq data (GSE118829). *PDIA3* expression in Tn and Tem from healthy (**A**) and RA-affected (**B**) individuals. (**C**) *PDIA3* expression in Tn and memory CD4 T cells (Tm) of RA patients from single-cell RNA sequencing data (GSE159117). Statistical significance was calculated by unpaired Student's t test. *p<0.05, ****p<0.0001. ns, not significant.
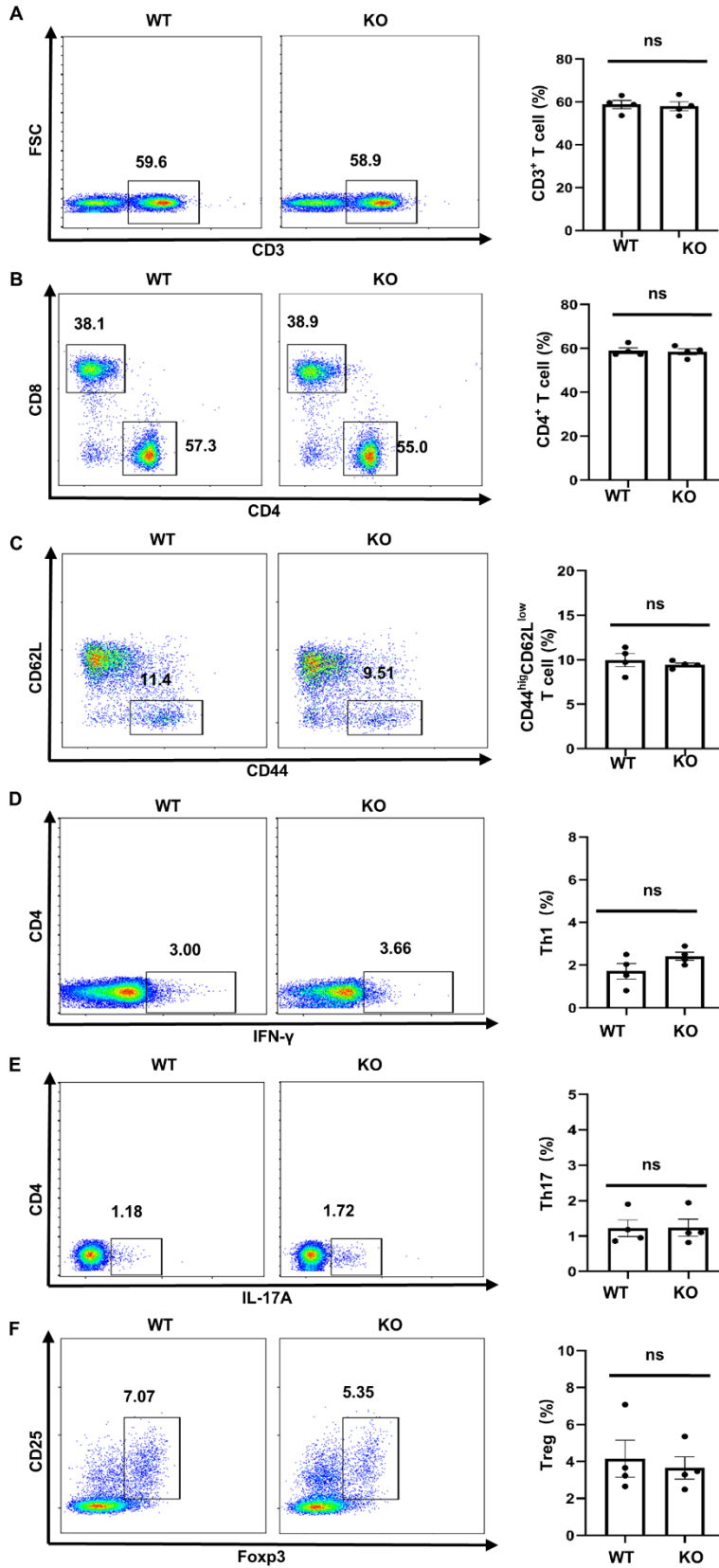
Fig. S2. Physiological T cell profiling in WT and KO mice. Spleens were harvested from 10-week-old WT and KO mice and subjected to flow cytometry analysis. Frequencies of (**A**) CD3$^+$ T cells, (**B**) CD4$^+$ T cells, (**C**) CD4$^+$CD44$^+$CD62L^{low}CD44^{high} T cells, (**D**) CD4$^+$IFN-γ^+ (Th1), (**E**) CD4$^+$IL-17A$^+$ (Th17) and (**F**) CD4$^+$Foxp3$^+$ (Treg) subsets are shown as representative dot plot graphs. Data are expressed as mean ± SEM (n=4 per group) and are representative of three independent experiments. Statistical significance was calculated by unpaired Student's t test. *p<0.05, **p<0.01, ***p<0.001. ns, not significant.
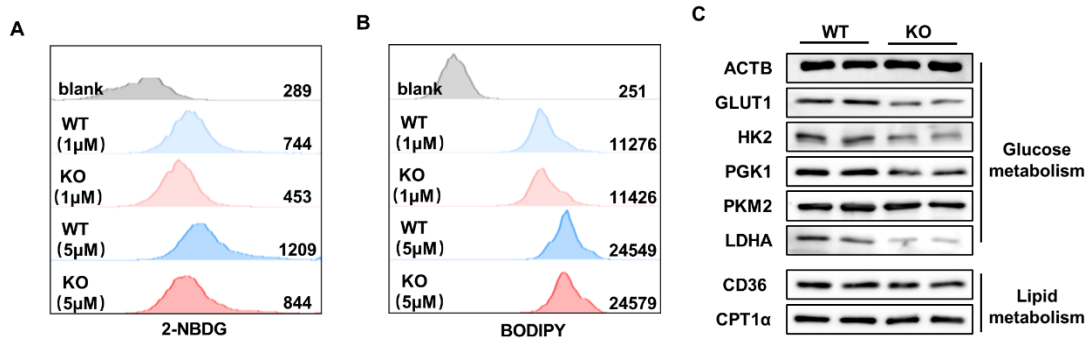
Fig. S3. The glucose and lipid metabolic phenotype in WT and KO CD4 T cells. CD4 T cells isolated from WT and KO mice were activated by plate-coated anti-CD3 and anti-CD28 antibodies for 48 h. (**A and B**) Glucose and lipid uptake was evaluated by measuring 2-NBDG and BODYPY fluorescence intensity using flow cytometry, respectively. (**C**) The expression levels of key molecules involved in glucose and lipid metabolism were determined by Western blot.
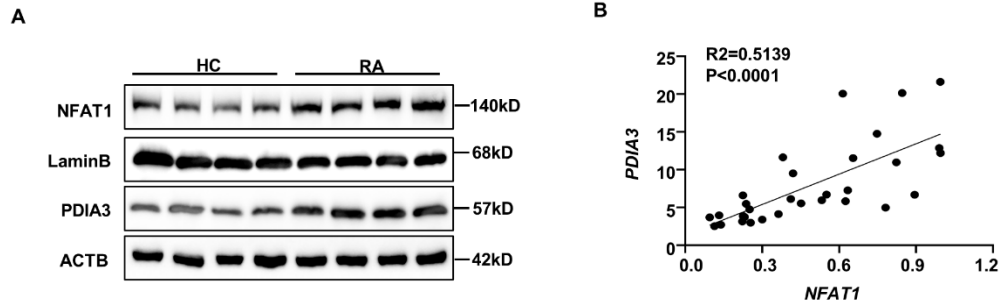
Fig. S4. The correlation between NFAT1 and PDIA3 expression levels in RA-derived CD4 T cells. (**A**) The expression levels of NFAT1 and PDIA3 were determined in CD4 T cells from healthy individuals and RA patients by Western blot. (**B**) The correlation between *PDIA3* and *NFAT1* mRNA levels in CD4 T cells from RA (N=31).
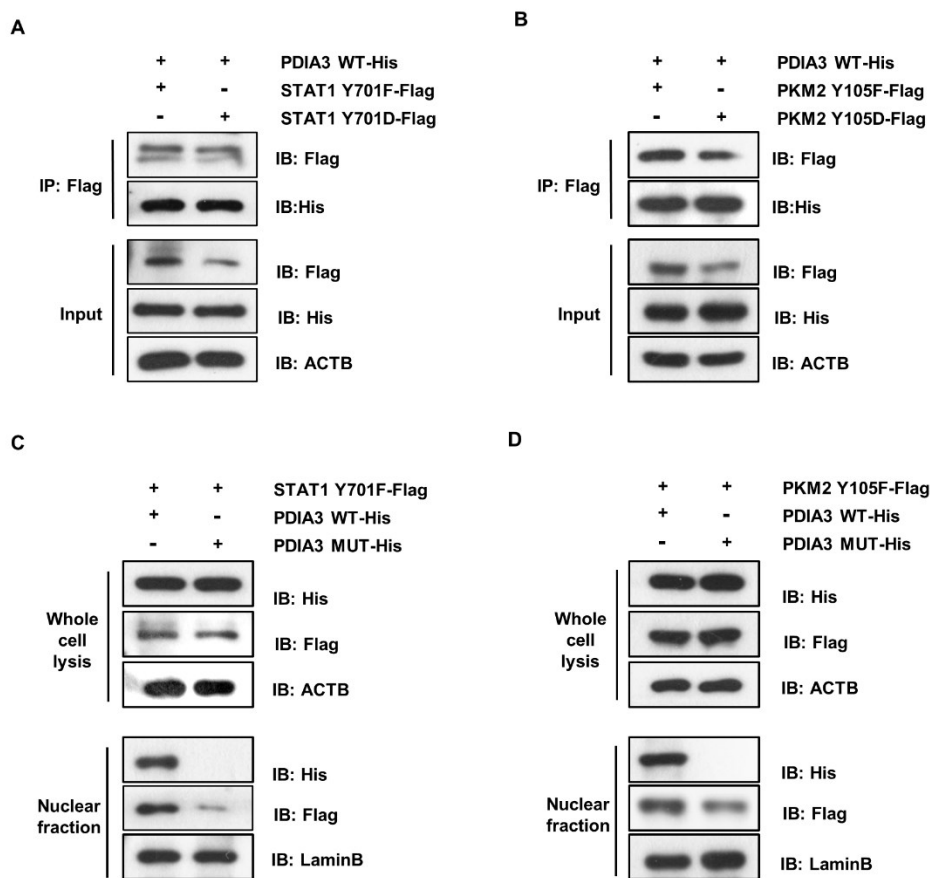
Fig. S5. PDIA3 interacts with STAT1 and PKM2 and functions as a nuclear transporter.

(**A**) HEK 293T cells were transfected with His tag-labeled wild-type *Pdia3* plasmid (PDIA3 WT-His) combined with Flag-labeled STAT1-Y701D (STAT1 Y701D-Flag) or STAT1-Y701F (STAT1 Y701F-Flag) plasmid for 48h and then subjected to Co-IP by anti-Flag antibody. (**B**) HEK 293T cells were transfected with PDIA3 WT-His plasmid combined with Flag-labeled PKM2-Y105D or PKM2-Y105F plasmid and then subjected to Co-IP by anti-Flag antibody. (**C**) HEK 293T cells were transfected with PKM2-Y105F plasmid combined with PDIA3 WT-His plasmid or STAT1-Y701F and then subjected to Co-IP by anti-Flag antibody. (**D**) HEK 293T cells were transfected with PDIA3 WT-His

combined with Flag-labeled PKM2-Y105D or PKM2-Y105F and then subjected to Co-IP by anti-Flag antibody.
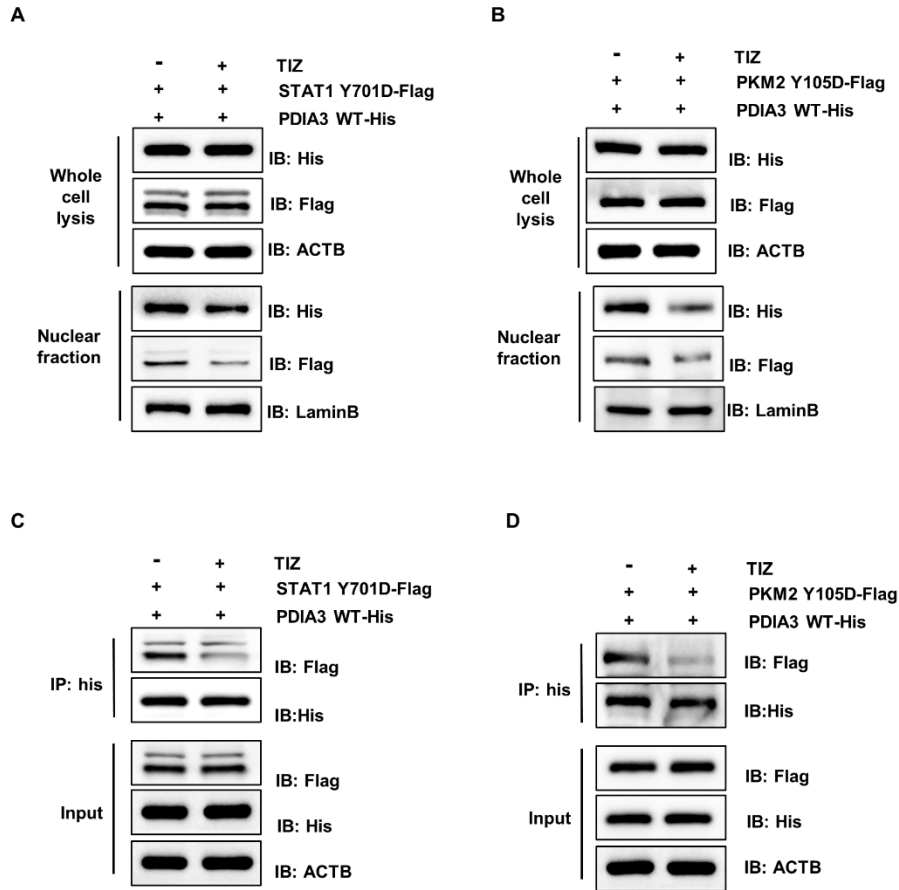
Fig. S6. The molecular mechanisms underlying the therapeutic effect of PDIA3 inhibitor Tizoxanide. HEK 293T cells were transfected with indicated plasmids, and Tizoxanide (TIZ) was administered 6 hours post-transfection. (**A and B**) The impact of TIZ on PDIA3-mediated nuclear transport of STAT1(A) and PKM2 (B). (**C and D**) The disruptive effect of TIZ on the interaction between PDIA3 and STAT1(C) or PKM2 (D).